Dalton Transactions

ROYAL SOCIETY OF CHEMISTRY

PAPER

View Article Online
View Journal | View Issue

Cite this: *Dalton Trans.*, 2026, **55**, 1915

Design of boron-decorated bimetallic iron complexes related to the active site of [FeFe]-hydrogenases and reactivity with hydride donors

Ines Bennour, Victor Monnot, Philippe Schollhammer* and Lucile Chatelain *

The reactivity of the 1,2-dithiolene diiron complexes $[Fe_2(\mu\text{-}SCH{=}C(Ph)S)(PR_3)_n(CO)_{6-n}]$ (n = 0, or n = 1, R = Me or n = 1, 2, R = Ph) with the reagent $HB(C_6F_5)_2$ is described. With the hexacarbonyl precursor, the reaction gives an anti-Markovnikov addition product $[Fe_2(\mu\text{-}SCH(B(C_6F_5)_2)\text{-}CH(Ph)S)(CO)_6]$. This represents a rare example of a diiron complex functionalized with a Lewis acidic borane, which has been characterized by spectroscopic measurements (NMR and IR), while an adduct with MeCN has been crystallographically analyzed. Starting from the mono-PMe_3 complex, the hydroboration is complicated by the formation of different isomers, while no hydroboration is observed with PPh_3 derivatives. In the latter case, the phosphane ligand is trapped by the boron atom. The reactivity of the diiron complexes functionalized with a Lewis acid group, $-B(C_6F_5)_2$, has been investigated toward dihydrogen and the hydride donor species $Na[HBEt_3]$. With a second equivalent of $HB(C_6F_5)_2$, a tetra-iron assembly $\{[Fe_2(\mu\text{-}SCH(BH(C_6F_5))\text{-}CH(Ph)S)(CO)_6]\}_2$ is formed selectively from $[Fe_2(\mu\text{-}SCH(B(C_6F_5)_2)\text{-}CH(Ph)S)(CO)_6]$ through a rearrangement of substituents around the boron atoms.

Received 2nd December 2025,
Accepted 16th December 2025

DOI: 10.1039/d5dt02885j

rsc.li/dalton

Introduction

The chemistry of Frustrated Lewis Pairs (FLPs) has been extensively developed since 2006, when the first phosphane–borane system capable of cleaving the H–H bond was reported.[1] Among the numerous reported examples, Transition Metal Frustrated Lewis Pairs (TMFLPs) have shown great potential due to the versatility of the coordination environment and the electronic properties of the metallic centres, which can act as acids or bases depending on their oxidation state and environment.[2,3] Notably, the active site of [FeFe]-hydrogenases, metalloenzymes that efficiently catalyse the reversible conversion of H^+ to H_2, has been described as a TMFLP formed by the basic amine of the azadithiolate ligand and the acidic $[Fe^I–Fe^{II}]$ center.[4,5] While many studies on bioinspired $\{Fe_2S_2\}$ complexes have reported their activity toward the hydrogen evolution reaction (HER),[6–8] H_2 cleavage or oxidation has been achieved much less frequently with such systems.[9–17] This limited reactivity may be attributed to the inherent instability of these organometallic complexes in the mixed-valent $[Fe^I–Fe^{II}]$ state.[18–25] To avoid this unstable redox state, we previously studied the ability of an inverted TMFLP polarity, based on a stable $[Fe^I–Fe^I]$ species and $B(C_6F_5)_3$ acting as a Lewis base and acid, respectively, to achieve heterolytic H_2 cleavage.[26] These examples of H_2 activation have been described as the first TMFLPs with a Lewis base constructed from a dinuclear iron complex. In our quest to investigate the reactivity between an $\{Fe_2S_2\}$ complex and a Lewis acidic borane, we seek to introduce a borane moiety into the second coordination sphere of a diiron complex. While pendant borane Lewis acids in the second coordination sphere or Z-type ligands are known in the literature to allow metal–ligand cooperativity,[27–30] favouring difficult transformations (H–H activation,[31–37] CO and CO_2 reduction,[38–40] N_2H_4 cleavage[41] or C–H activation[42]), only one structural study of $\{Fe_2S_2\}$ complexes containing a trisubstituted boron atom in the second coordination sphere was reported in 1986: $[Fe_2(\mu\text{-}SB(L)S)(CO)_6]$ (L: 2,2,6,6-tetramethylpiperidine) and $[Fe_2(\mu\text{-}SB(NMe_2)\text{-}B(NMe_2)S)(CO)_6]$.[43] Since then, the literature has revealed only Lewis adducts resulting from the interaction between the boron atom and oxygen,[44] nitrogen[45–47] or phosphorus[48] atoms of diiron dithiolate complexes.

To achieve the functionalization of $\{Fe_2S_2\}$ moieties with a borane group in the secondary coordination sphere, two strategies have been envisioned: one using Z-type ligands and the other using hydroboration of a ligand supported by the diiron complex. In the first case, in our hands, the reported PBP Z-type ligands could not be coordinated to diiron complexes.[49,50] In the second case, surprisingly, a hydroboration reaction of a C=C bond has never been reported for

UMR CNRS 6521 Chimie, Electrochimie Moléculaires et Chimie Analytique, Univ. Brest, 6 Avenue Victor le Gorgeu, CS93837, Brest-Cedex 3, 29238, France.
E-mail: philippe.schollhammer@univ-brest.fr, lucile.chatelain@univ-brest.fr

dinuclear complexes, and more precisely, for diiron dithiolate complexes, while it has been reported with $HB(C_6F_5)_2$ on mononuclear complexes of group VIII (Fe and Ru).[51–55]

In this work, we report the reactivity of the hexacarbonyl 1,2-dithiolene diiron complex $[Fe_2(\mu\text{-SCH=C(Ph)S})(CO)_6]$ with $HB(C_6F_5)_2$. The impact of electronic density on the diiron core during hydroboration has been examined through substitution of one or two carbonyl ligands by phosphane ligands such as PMe_3 or PPh_3. These first examples of diiron/borane assemblies have been characterized by spectroscopic techniques (IR and NMR). Their reactivity with H_2, $Na[HBEt_3]$ and $HB(C_6F_5)_2$ is also reported.

Results and discussion

Synthesis of the $\{Fe_2S_2\}$ precursors

The complex $[Fe_2(\mu\text{-SCH=C(Ph)S})(CO)_6]$ (**1**) is synthesized according to the published procedure of Seyferth and co-workers, through the nucleophilic addition of lithium acetylide to the disulfide complex $[Fe_2(\mu\text{-}S_2)(CO)_6]$.[56]

In our hands and even after purification, around 5% of a 1,1′-dithiolene isomer, $[Fe_2(\mu\text{-SC(=CH(Ph))S})(CO)_6]$ (**1′**), is present alongside the 1,2-dithiolene product (Scheme 1). The mixture of the two isomers is used as a precursor for introducing PPh_3 and PMe_3 ligands in the coordination sphere of iron. The complexes $[Fe_2(\mu\text{-SCH=C(Ph)S})(PPh_3)_x(CO)_{6-x}]$ (x = 1, 2) (**2** and **3**) are synthesized according to a recently published procedure,[57] in good yields (66–70%), from the successive substitution of CO by PPh_3. In contrast, the synthesis of the complex $[Fe_2(\mu\text{-SCH=C(Ph)S})(PMe_3)(CO)_5]$ (**4**) occurs only in low yield (~19%) after the addition of one equivalent of PMe_3 to a toluene solution of **1** (Scheme 1).

The crystallographic structure of **4** (Fig. 1) reveals an $\{Fe_2S_2\}$ butterfly core, with each iron centre in a distorted square pyramidal geometry. The Fe–Fe bond distance of 2.4702(5) Å is in agreement with similar X-ray structures reported for monophosphane substituted diiron 1,2-dithiolene complexes (ranging from 2.4772(6) to 2.5047(6) Å).[58,59] The C=C bond length (1.332(3) Å) is consistent with a double bond.[59] The PMe_3 ligand is located in the apical position of the iron atom, with an Fe–P bond distance of 2.2143(7) Å in the range of previously reported examples (2.1651(9)–2.2496(8) Å).[58,59]

A typical pattern for mono-substituted derivatives $[Fe_2(\mu\text{-dithiolate})(CO)_5(L)]$ is observed in the IR spectrum of **4** in the ν_{CO} region (Table 1 and Fig. S6).[57–59] The wavenumber of the bands related to the CO stretch are lower than those of complex **1**, in agreement with the increased π-back-donation of the iron atom to the π* anti-bonding orbital of the CO ligand after the phosphane coordination. The ^1H and $^{13}C\{^1H\}$ NMR spectra in CD_2Cl_2 agree with the structure determined by X-ray diffraction (Fig. S7–S9). One broad resonance is observed in

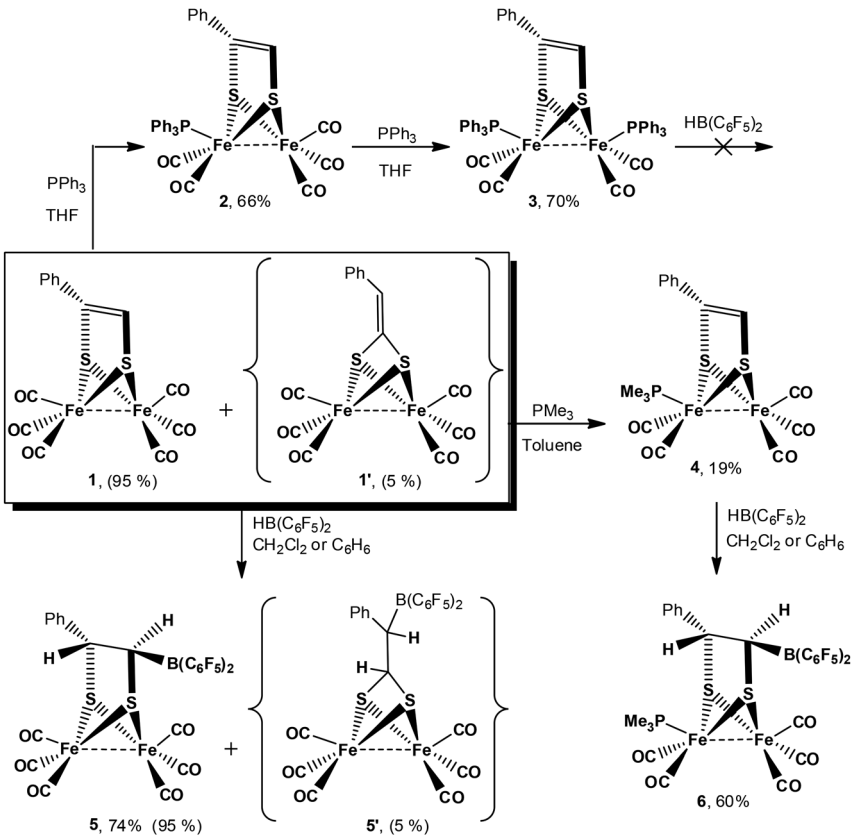

Scheme 1 Synthesis of complexes **2–6** (the percentage in parentheses refers to the amount of the isomer in the isolated solid).

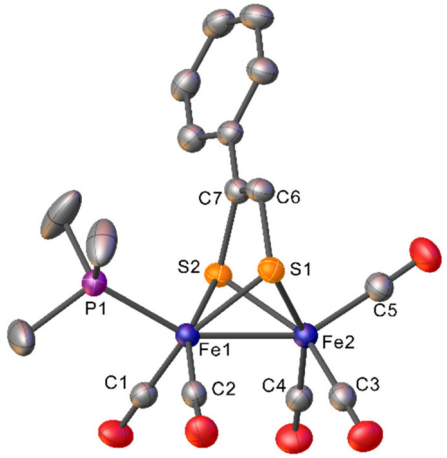

Fig. 1 Molecular structure of $[Fe_2(\mu\text{-}SCH{=}C(Ph)S)(PMe_3)(CO)_5]$ (**4**) with thermal ellipsoids at 40% probability (hydrogen atoms are omitted for clarity). Colour code: carbon in grey, oxygen in red, iron in dark blue, sulfur in orange, and phosphorus in purple. Bond distances: $Fe{-}S_{mean}$, 2.279(14) Å; Fe–P, 2.2143(7) Å; $Fe{-}C_{mean}$, 1.783(14) Å; and CO_{mean}, 1.142 (4) Å.

Table 1 IR spectroscopic data for complexes **1–6** in CH_2Cl_2

Complex	ν_{CO} (cm^{-1})
1	2079, 2043, 2003
4	2048, 1989, 1975 (sh), 1932
5	2072, 2031, 2000, 1988 (sh)
$\mathbf{5^{H-Na}}$	2069, 2027, 1999, 1983 (sh)
6	2044, 1989, 1971, 1932
$\mathbf{6^{H-Na}}$	2032, 1974, 1957 (sh), 1889 (w)

the $^{31}P\{^1H\}$ NMR (CD_2Cl_2) spectrum, which splits into three singlets (20.5, 27.9 and 28.1 ppm) upon decreasing the temperature to 223 K. These signals are assigned to the three isomers of **4** according to the apical or basal position of PMe_3 with respect to the orientation of the phenyl group on the dithiolene ligand (Fig. S1, left). In contrast to **1**, compound **4** is isolated without traces of the 1,1′-dithiolene isomer. Moreover, in contrast to the reactivity of **1** with PPh_3, affording mono- and di-substituted complexes $[Fe_2(\mu\text{-}SCH{=}C(Ph)S)(PPh_3)_x(CO)_{6-x}]$ (x = 1, 2) (**2** and **3**) with moderate heating at 40 °C to favour two CO substitutions,[57] the replacement of a second CO with PMe_3 in **4** failed to produce $[Fe_2(\mu\text{-}SCH{=}C(Ph)S)(PMe_3)_2(CO)_4]$ even with thermal or photochemical activation. Attempts to substitute PPh_3 ligands in $[Fe_2(\mu\text{-}SCH{=}C(Ph)S)(PPh_3)_2(CO)_4]$ (**3**) with two equivalents of PMe_3 do not yield the desired compound but a mixture of products arising from degradation of the diiron core. Such degradation may be linked to Fe–Fe bond cleavage, which has already been reported for related 1,2-dithiolene diiron complexes substituted with $P(OMe)_3$ ligands, leading to the formation of mono-iron complexes.[59,60] The reactivity of the four complexes **1–4** is then examined towards the hydroboration reagent $HB(C_6F_5)_2$.

Hydroboration reactions

The hydroboration reactions are performed with the addition of 1.2 equivalents of $HB(C_6F_5)_2$ to a CH_2Cl_2 or benzene solution of complexes **1**, **2**, **3** or **4**. The evolution of the reaction is followed by ^1H NMR measurements. In the case of **1**, the disappearance of the singlet related to the *H*C = resonance is observed, and two main novel signals appear in the ^1H NMR spectrum, related to the anti-Markovnikov addition of HB$(C_6F_5)_2$ to the C=C bond (Fig. 2 and S10). Two isomeric complexes, $[Fe_2(\mu\text{-}SCH(B(C_6F_5)_2)\text{-}CH(Ph)S)(CO)_6]$ (**5**) and $[Fe_2(\mu\text{-}SCH(\text{–}CH(Ph)(B(C_6F_5)_2))S)(CO)_6]$ (**5′**), are formed in a 95/5% ratio from **1**/**1′**. The ^1H NMR spectrum of **5** in C_6D_6 displays two doublets at 3.3 and 3.5 ppm ($^3J_{HH}$ = 8 Hz) corresponding to the two hydrogen atoms of the bridging ligand –SC*H*B-C*H*(Ph)S–. The two doublets at 4.9 and 5.4 ppm ($^3J_{HH}$ = 11 Hz) are attributed to the minor isomer **5′** containing the –SCH(C*H*BPh)S– bridge. Aromatic protons are found between 7.3 and 7.4 ppm. The $^{13}C\{^1H\}$ spectrum reveals the disappearance of the characteristic resonances of the C=C bond (at 134.4 and 161.7 ppm)[56] and the appearance of upfield resonances. Notably, a two-dimensional HSQC ^{13}C–^1H NMR experiment supports the main formation of **5** with the –SC*H*B-C*H*(Ph)S– bridge and **5′** with the bridging –SCH(C*H*BPh)S– ligand as a minor species (Fig. S12). The two aromatic $-C_6F_5$ cycles are equivalents as the $^{19}F\{^1H\}$ NMR spectrum reveals only three multiplets for the *ortho*-, *meta*- and *para*-positions (Fig. S13). Finally, the broad resonance observed at 62.9 ppm in the $^{11}B\{^1H\}$ NMR spectrum is characteristic of sp^2 hybridized boron (Fig. S14). X-ray quality single crystals of $\mathbf{5^{MeCN}}$ grew in a 1 : 3 acetonitrile/toluene solution. The crystallographic data unambiguously confirm the structure of the complex $[Fe_2(\mu\text{-}SCH(B(C_6F_5)_2(MeCN))\text{-}CH(Ph)S)(CO)_6]$ ($\mathbf{5^{MeCN}}$) (Fig. 3). It consists of

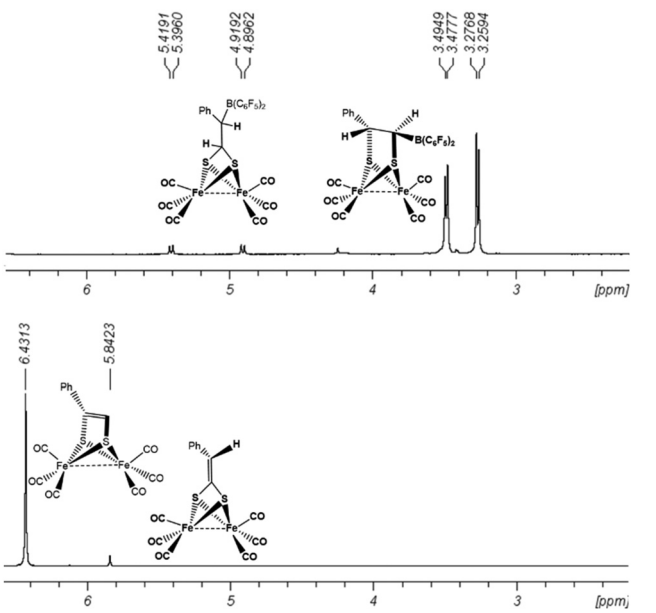

Fig. 2 ^1H NMR (400 MHz, 298 K, C_6D_6) spectrum of compounds **1**/**1′** before (bottom) and after (top) addition of 1.2 equivalents of $HB(C_6F_5)_2$.

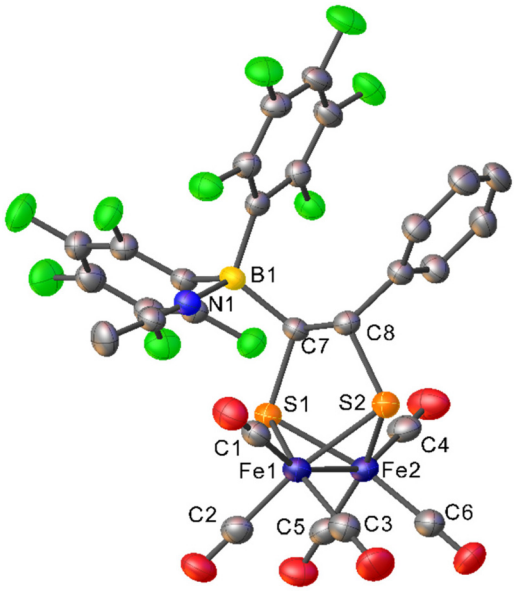

Fig. 3 Molecular structure of $[Fe_2(\mu\text{-SCH}(B(C_6F_5)_2(MeCN))\text{-CH(Ph)S})(CO)_6]\cdot(toluene)_{2.5}$ ($\mathbf{5}^{\mathbf{MeCN}}$)$(toluene)_{2.5}$ with thermal ellipsoids at 40% probability (hydrogen atoms and co-crystallized solvent molecule are omitted for clarity). Colour code: carbon in grey, oxygen in red, iron in dark blue, sulfur in orange, boron in yellow, fluorine in light green, and nitrogen in blue. Bond distances: Fe–S_{mean}, 2.251(7) Å; Fe–C_{mean}, 1.789 (5) Å; and CO_{mean}, 1.142(4) Å.

a butterfly $\{Fe_2S_2\}$ core, and the Fe–Fe bond length is 2.4849(6) Å, shorter than the one found in $[Fe_2(\mu\text{-edt})(CO)_6]$ (edt^{2-}: 1,2-ethanedithiolate) (2.499(8) Å)[61–63] but longer than that in complex **1** (2.4665(6) Å).[57] The dithiolene C=C bond length (1.317(4) Å) observed in complex **1** is significantly longer than that in complex $\mathbf{5}^{\mathbf{MeCN}}$, in agreement with a single bond (d_{C7C8} 1.527(3) Å compared to 1.505(2) Å in $[Fe_2(\mu\text{-edt})(CO)_6]$).[61–63] An acetonitrile molecule is bound to the boron atom and the two $-C_6F_5$ groups are inequivalent, in agreement with the $^{19}F\{^1H\}$ and $^{11}B\{^1H\}$ NMR spectra recorded in CD_3CN (Fig. S16 and S17). The IR spectrum of the CH_2Cl_2 solution of **5**/**5′** displays, in the ν_{CO} region, a typical pattern for hexacarbonyl derivatives, with three strong bands at 2072, 2031, and 2000 cm^{-1} and a shoulder at 1988 cm^{-1}, slightly shifted compared to those of complex **1** (Table 1 and Fig. S3). In comparison, the non-functionalized complex $[Fe_2(\mu\text{-edt})(CO)_6]$ displays IR stretching bands for carbonyl ligands at 2076, 2036, 2000 and 1994 cm^{-1}.[62] These IR data suggest that there is no electron-withdrawing effect of the borane on the dithiolate bridge.

The reaction of complex **4** with $HB(C_6F_5)_2$, in the absence of the 1,1′-dithiolene isomer in solution, leads to the sole complex $[Fe_2(\mu\text{-SCH}(B(C_6F_5)_2)\text{-CH(Ph)S})(PMe_3)(CO)_5]$ (**6**) (Scheme 1).

Its ^1H NMR spectrum in C_6D_6 reveals the presence of several isomers. Six broad doublets are found between 3.3 and 3.7 ppm, most probably corresponding to three different isomers, in agreement with the signals of the PMe_3 group found in the ^1H and $^{31}P\{^1H\}$ NMR spectra (multiplets at 0.7–0.8 ppm and 16.8–24.1–24.3, respectively) (Fig. S18 and S19). The resonances observed in the $^{31}P\{^1H\}$ NMR spectrum recorded in CD_2Cl_2 split upon decreasing temperature to 223 K into five signals, related to the respective position of the PMe_3 ligand (Fig. S1, left) and the anti-Markovnikov addition of Piers' reagent to the C=C bond (Fig. S1, right). For complex **6**, a broad resonance around 60 ppm is observed in the $^{11}B\{^1H\}$ NMR spectrum for the three-coordinate boron atom (Fig. S20). The $^{19}F\{^1H\}$ NMR spectrum reveals three main resonances related to equivalents of $-C_6F_5$ (Fig. S21). The IR spectra of **5** and **6** indicate that the hydroboration of the complexes **1** and **4** induces a small shift of ν_{CO} to lower wavenumbers (Table 1 and Fig. S6).

The hydroboration of complexes $[Fe_2(\mu\text{-SCH=C(Ph)S})(PPh_3)_x(CO)_{6-x}]$ (x = 1, 2) (**2** and **3**) has also been performed with $HB(C_6F_5)_2$. Surprisingly, in both cases, the formation of the adduct $PPh_3\text{-}BH(C_6F_5)_2$ (resonances on the $^{31}P\{^1H\}$ and $^{11}B\{^1H\}$ NMR (CD_2Cl_2) spectra at 12 ppm and −23.9 ppm, respectively) is observed (Fig. S23).[64] This difference in reactivity is probably due to a stronger coordination of PMe_3 towards the iron centre compared to PPh_3, preventing the decomposition of **4**.

Finally, the hydroboration reaction, which has no literature precedent for an $\{Fe_2S_2\}$ complex, was found to be effective in introducing a borane group into the second coordination sphere of the diiron sites in complexes **1** and **4**, yielding **5** and **6**. Several types of reactivity between Lewis acids and organometallic iron complexes have been reported, including oxidative addition and binding to thiolate ligands in mononuclear iron complexes,[64,65] as well as coordination to the CO ligand in an $\{Fe_2S_2\}$ complex.[44] However, such reactivities are unlikely for hexa- and pentacarbonyl $\{Fe_2S_2\}$ complexes in the absence of thermal or photochemical activation, leaving hydroboration of C=C as the most probable reaction pathway.

The reactivity of complexes **5** and **6** with H_2, $HB(C_6F_5)_2$ and $HBEt_3^-$ has then been considered in order to localize their acidic subsite.

Reactivity of 5 and 6 with H_2, $HB(C_6F_5)_2$ and $HBEt_3^-$

The obtention of the functionalized complexes **5** and **6** containing a bimetallic $\{Fe^I\text{–}Fe^I\}$ core and a Lewis acidic group, *i.e.* $-B(C_6F_5)_2$, led us to investigate their reactivity towards H_2 and hydride donors. Unlike the FLPs formed by the complexes $[Fe_2(\mu\text{-pdt})L^{\#}(CO)_4]$ (pdt^{2-}: 1,3-propanedithiolate; $L^{\#}$: 1,2-bis(dimethylphosphino)ethane = κ^2-dmpe or 2 PMe_3) and the Lewis acid $B(C_6F_5)_3$,[26] no evolution is observed when solutions of **5** or **6** are exposed to H_2 (1 atm). This indicates that compounds **5** and **6** do not allow the cleavage of the H–H bond. This may be partly attributed to the poor geometric orientation of the borane group with respect to the diiron site, as well as an unfavourable electronic balance between the Lewis acid and base components. The Lewis acidity of the borane complex cannot be easily increased, as the borane group $-B(C_6F_5)_2$ introduced into the second coordination sphere of the diiron is among the stronger Lewis acids.[66] Moreover, increasing the basicity of the bimetallic iron site by replacing CO with

PMe_3 has so far been limited to mono-substitution reactions, while attempts to substitute two CO ligands using chelating diphosphanes such as dmpe or dppe (1,2-bis(diphenylphosphino)ethane) have been unsuccessful in our hands.

The reactivity of **5** and **6** has been then considered towards hydride donors such as $Na[HBEt_3]$. The addition of one equivalent of this reagent to complexes **5** and **6** in toluene leads to complexes $\mathbf{5}^{\mathbf{H-Na}}$ and $\mathbf{6}^{\mathbf{H-Na}}$ (Scheme 2). A solution of THF/toluene afforded single crystals of $\mathbf{5}^{\mathbf{H-Na}}.(THF)_3$. The analysis of the XRD data revealed the presence of the expected diiron complex with a borate $-C_{dithiolate}BH(C_6F_5)_2^-$ group and a sodium counter-cation surrounded by THF molecules. While the poor crystallographic data due to crystallographic twinning prevents a bond distance analysis, the connectivity of atoms is without ambiguity (Fig. S2). The addition of the hydride to the boron atom of complexes **5** and **6** leads to a decrease in ν_{CO} wavenumbers and the retention of the respective hexa- and pentacarbonyl diiron ν_{CO} patterns (Table 1 and Fig. S4 and S6), which is expected due to the electron enrichment of the dithiolate bridge.

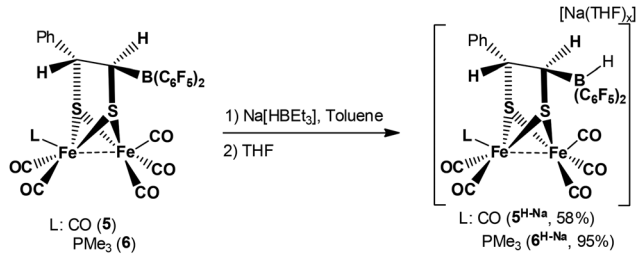

Scheme 2 Synthesis of complexes $\mathbf{5}^{\mathbf{H-Na}}$ and $\mathbf{6}^{\mathbf{H-Na}}$.

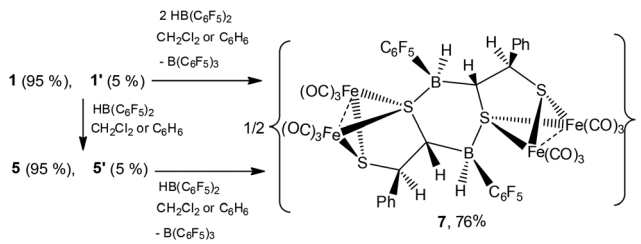

Scheme 3 Synthesis of complex **7**.

The borohydride resonance could not be assigned in the ^1H NMR spectrum of $\mathbf{5}^{\mathbf{H-Na}}$ and $\mathbf{6}^{\mathbf{H-Na}}$ in CD_2Cl_2, but a singlet and a doublet ($^1J_{BH}$ = 83–86 Hz) around −19 ppm are respectively detected in the $^{11}B\{^1H\}$ and the ^{11}B NMR spectra (Fig. S25 and S30). This observation confirms unambiguously the presence of the hydride in the borate group in accordance with the reported chemical shift of similar species.[67–69] As for **6**, a decrease in temperature from 298 to 223 K results in the splitting of the signal observed for PMe_3 in the $^{31}P\{^1H\}$ NMR spectrum of $\mathbf{6}^{\mathbf{H-Na}}$ into two singlets, which are assigned to two isomers (Fig. S28). The formation of the borohydride species $\mathbf{5}^{\mathbf{H-Na}}$ and $\mathbf{6}^{\mathbf{H-Na}}$ confirms that the acidic site of compounds **5** and **6** is, as expected, localized on the borane group.

In order to further explore the properties of **5** and **6**, their reactivity has been investigated with $HB(C_6F_5)_2$, in which the polarization of the B–H bond is between those of H_2 and Na[$HBEt_3$]. The addition of an equivalent of $HB(C_6F_5)_2$ to complexes **5** and **6** has been performed in C_6D_6 solution. In the case of **5**, the crystallization of the major product of the reaction $\{[Fe_2(\mu\text{-}SCH(BH(C_6F_5))\text{-}CH(Ph)S)(CO)_6]\}_2$ (**7**) occurs directly in the reaction mixture and after 7 days the crystals are recovered in 76% yield (Scheme 3). Interestingly, the direct addition of two equivalents of $HB(C_6F_5)_2$ to complex **1** in C_6D_6 also leads to the clean formation of **7**. X-ray diffraction analysis of crystals of **7** revealed an unexpected structure containing a

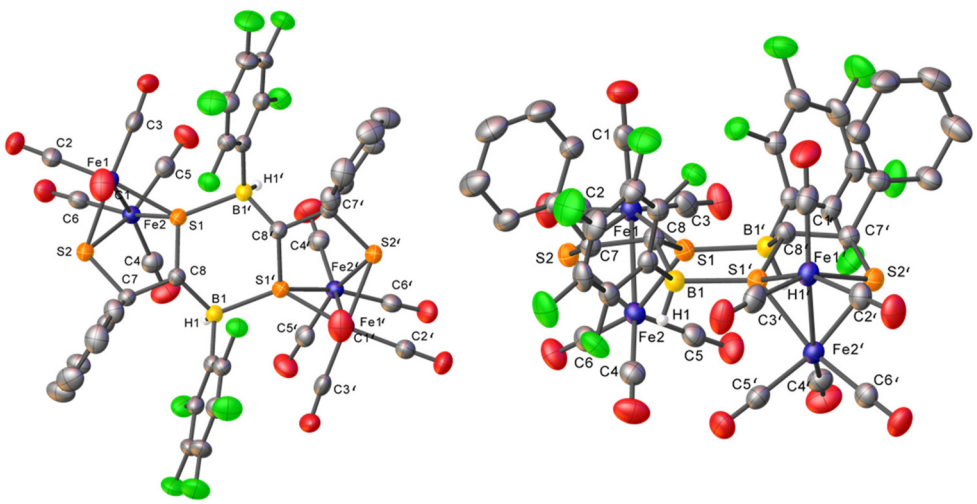

Fig. 4 Top and side views of the molecular structures of $\{[Fe_2(\mu\text{-}SCH(BH(C_6F_5))\text{-}CH(Ph)S)(CO)_6]\}_2(C_6H_6)_3$ (**7**)$(C_6H_6)_3$ with thermal ellipsoids at 40% probability (hydrogen atoms, except H1 bound to B1, and co-crystallized solvent molecule are omitted for clarity). Atoms with labels are obtained from the (1 − *x*, +*y*, 3/2 − *z*) symmetry. Colour code: carbon in grey, oxygen in red, iron in dark blue, sulfur and sodium in orange, boron in yellow, and fluorine in light green. Bond distances: $Fe\text{–}S_{1(B)mean}$, 2.2147(7) Å; $Fe\text{–}S_{2mean}$, 2.2552(7) Å; $Fe\text{–}C_{mean}$, 1.804(3) Å; CO_{mean}, 1.136(3) Å; and $S_1\text{–}B$ 1.985(3) Å.

tetra-iron complex (Fig. 4). Only half of the molecule is present in the asymmetric unit. Two $\{Fe_2S_2\}$ butterfly cores are connected together by two symmetrical tetravalent borohydrides; each of them is linked to one carbon of a dithiolate bridge, one $-C_6F_5$ group, one hydrogen and one sulfur atom of a second dithiolate diiron entity. This forms a six-membered cycle –C–B–S–C–B–S– with a boat conformation. The Fe–Fe bond distance (2.5164(5) Å) is longer than those in complex $\mathbf{5}^{\mathbf{MeCN}}$ (2.4849(6) Å) and other $\{Fe^{I}–Fe^{I}\}$ 1,2-ethanedithiolate derivatives (2.499(8) Å).[61–63]

This elongated distance may be explained by the coordination of one sulfur atom to a boron atom. The S_1–B bond distance of 1.985(3) Å related to the dithiolate bridge is in agreement with the related boron-sulfur bond length found in the reported compound $[Cp^*Fe(1,2\text{-}Ph_2P(C_6H_4)S)(HB(C_8H_{14}))]$ (1.949(5) Å).[65] The Fe–S bond distances, Fe–S_1 and Fe–S_2, are significantly asymmetric (average distances of 2.2147(7) and 2.2552(7) Å, respectively) in contrast to the more symmetrical complex $\mathbf{5}^{\mathbf{MeCN}}$ (Fe–S bond ranging from 2.2443(8) to 2.2590(8) Å). Adding a second equivalent of $HB(C_6F_5)_2$ causes a redistribution of the boron substituents, yielding a tetrasubstituted group "–BH(C)(C_6F_5)S". This leads to the release of a $B(C_6F_5)_3$ molecule into solution, observed in NMR spectra (Fig. S34). The $^{11}B\{^1H\}$ and $^{19}F\{^1H\}$ NMR spectra of crystals of **7** after dissolution in CD_2Cl_2 (Fig. S31–S33) agree with a negatively charged boron atom (−7.1 ppm on $^{11}B\{^1H\}$ NMR) and inequivalent *ortho* and *meta* fluorine atoms in the $-C_6F_5$ group. The carbonyl bands are significantly shifted to higher frequencies (2084, 2054, and 2019 cm^{-1}) compared to compound **1** or **5**, in agreement with the electronic donation of S_1 to the boron atom (Fig. S4).

A proposed mechanism is depicted in Fig. S1b in the SI to explain the formation of **7**. We hypothesize that the first step arises from the interaction of $HB(C_6F_5)_2$ with the sulfur atom of the dithiolate bridge,[70] followed by disproportionation between boron atoms,[71–73] and a cyclisation step that makes the final compound more stable.

In contrast, the addition of an equivalent of $HB(C_6F_5)_2$ to **6** in C_6D_6 does not yield a single species but rather a multitude of species, as observed in the $^{31}P\{^1H\}$ and the $^{19}F\{^1H\}$ NMR spectra (Fig. S36 and S37).

Conclusions

Two $\{Fe_2S_2\}$ complexes related to the active site of [FeFe] hydrogenases have been successfully functionalized with a Lewis acidic borane. The strategy of using hydroboration reaction allows the formation of intramolecular $\{Fe^{I}–Fe^{I}\}$/B complexes, in which a borane function is localized into the second coordination sphere of the two iron metals. While no FLP reactivity is observed with H_2, borane complexes react with hydride to form the expected borohydride species. These results demonstrate that the boron group acts as a Lewis acid and support our strategy to build the envisioned FLP by combining a homobimetallic iron complex with a borane function, respectively, playing the role of a Lewis base and Lewis acid. In order to favour H_2 activation, electronic and geometrical adjustments of the Lewis pair within such species are ongoing.

Conflicts of interest

There are no conflicts to declare.

Data availability

The data supporting this article have been included as part of the supplementary information (SI). Supplementary information: IR, NMR, crystallography, and ESI-MS. See DOI: https://doi.org/10.1039/d5dt02885j.

CCDC 2451917–2451920 contain the supplementary crystallographic data for this paper.[74a–d]

Acknowledgements

The authors thank L. Labous and Dr G. Simon, S. Cérantola, and F. Michaud for their help in recording ESI-MS, NMR and XRD experiments at the 'Service Général des Plateformes, Brest' (SGPLAT). L. C. thanks the ANR (Agence Nationale de Recherche) for funding the project JCJC OxySplit-H2 (ANR-20-CE07-0027-01). I. B. and L. C. acknowledge the support of the Region Bretagne for funding the project SAD ConvCatH.

References

1 G. C. Welch, R. R. S. Juan, J. D. Masuda and D. W. Stephan, *Science*, 2006, **314**, 1124–1126.
2 D. F. Wass and A. M. Chapman, in *Frustrated Lewis Pairs II: Expanding the Scope*, ed. G. Erker and D. W. Stephan, Springer, Berlin, Heidelberg, 2013, pp. 261–280.
3 N. Hidalgo, M. G. Alférez and J. Campos, in *Frustrated Lewis Pairs*, ed. J. Chris Slootweg and A. R. Jupp, Springer International Publishing, Cham, 2021, pp. 319–359.
4 R. M. Bullock and G. M. Chambers, *Philos. Trans. R. Soc., A*, 2017, **375**, 20170002.
5 F.-G. Fontaine and D. W. Stephan, *Philos. Trans. R. Soc., A*, 2017, **375**, 20170004.
6 D. Schilter, J. M. Camara, M. T. Huynh, S. Hammes-Schiffer and T. B. Rauchfuss, *Chem. Rev.*, 2016, **116**, 8693–8749.
7 G. Hogarth, *Coord. Chem. Rev.*, 2023, **490**, 215174.
8 T. Agarwal, N. Kumar, Ritu and S. Kaur-Ghumaan, *Electrochim. Acta*, 2024, 144852.
9 M. T. Olsen, B. E. Barton and T. B. Rauchfuss, *Inorg. Chem.*, 2009, **48**, 7507–7509.
10 J. M. Camara and T. B. Rauchfuss, *J. Am. Chem. Soc.*, 2011, **133**, 8098–8101.
11 J. M. Camara and T. B. Rauchfuss, *Nat. Chem.*, 2012, **4**, 26–30.

12 N. Wang, M. Wang, Y. Wang, D. Zheng, H. Han, M. S. G. Ahlquist and L. Sun, *J. Am. Chem. Soc.*, 2013, **135**, 13688–13691.
13 G. R. F. Orton, S. Belazregue, J. K. Cockcroft, F. Hartl and G. Hogarth, *J. Organomet. Chem.*, 2023, **991**, 122673.
14 S. Ghosh, G. Hogarth, N. Hollingsworth, K. B. Holt, S. E. Kabir and B. E. Sanchez, *Chem. Commun.*, 2013, **50**, 945–947.
15 M. Cheng, M. Wang, D. Zheng and L. Sun, *Dalton Trans.*, 2016, **45**, 17687–17696.
16 M. E. Ahmed, A. Nayek, A. Križan, N. Coutard, A. Morozan, S. Ghosh Dey, R. Lomoth, L. Hammarström, V. Artero and A. Dey, *J. Am. Chem. Soc.*, 2022, **144**, 3614–3625.
17 A. Nayek, R. K. Poria, M. E. Ahmed, S. Patra, S. G. Dey and A. Dey, *ACS Org. Inorg. Au*, 2025, **5**, 105–116.
18 M. Razavet, S. J. Borg, S. J. George, S. P. Best, S. A. Fairhurst and C. J. Pickett, *Chem. Commun.*, 2002, 700–701.
19 A. K. Justice, T. B. Rauchfuss and S. R. Wilson, *Angew. Chem., Int. Ed.*, 2007, **46**, 6152–6154.
20 T. Liu and M. Y. Darensbourg, *J. Am. Chem. Soc.*, 2007, **129**, 7008–7009.
21 M. L. Singleton, N. Bhuvanesh, J. H. Reibenspies and M. Y. Darensbourg, *Angew. Chem., Int. Ed.*, 2008, **47**, 9492–9495.
22 A. K. Justice, L. De Gioia, M. J. Nilges, T. B. Rauchfuss, S. R. Wilson and G. Zampella, *Inorg. Chem.*, 2008, **47**, 7405–7414.
23 C. M. Thomas, T. Liu, M. B. Hall and M. Y. Darensbourg, *Inorg. Chem.*, 2008, **47**, 7009–7024.
24 Ö. F. Erdem, L. Schwartz, M. Stein, A. Silakov, S. Kaur-Ghumaan, P. Huang, S. Ott, E. J. Reijerse and W. Lubitz, *Angew. Chem., Int. Ed.*, 2011, **50**, 1439–1443.
25 C.-H. Hsieh, Ö. F. Erdem, S. D. Harman, M. L. Singleton, E. Reijerse, W. Lubitz, C. V. Popescu, J. H. Reibenspies, S. M. Brothers, M. B. Hall and M. Y. Darensbourg, *J. Am. Chem. Soc.*, 2012, **134**, 13089–13102.
26 L. Chatelain, J.-B. Breton, F. Arrigoni, P. Schollhammer and G. Zampella, *Chem. Sci.*, 2022, **13**, 4863–4873.
27 A. Maity and T. S. Teets, *Chem. Rev.*, 2016, **116**, 8873–8911.
28 M. R. Elsby and R. T. Baker, *Chem. Soc. Rev.*, 2020, **49**, 8933–8987.
29 M. W. Drover, *Chem. Soc. Rev.*, 2022, **51**, 1861–1880.
30 J. A. Zurakowski, B. J. H. Austen and M. W. Drover, *Trends Chem.*, 2022, **4**, 331–346.
31 J. B. Bonanno, T. P. Henry, P. T. Wolczanski, A. W. Pierpont and T. R. Cundari, *Inorg. Chem.*, 2007, **46**, 1222–1232.
32 N. Tsoureas, Y.-Y. Kuo, M. F. Haddow and G. R. Owen, *Chem. Commun.*, 2010, **47**, 484–486.
33 W. H. Harman and J. C. Peters, *J. Am. Chem. Soc.*, 2012, **134**, 5080–5082.
34 S. K. Podiyanachari, R. Fröhlich, C. G. Daniliuc, J. L. Petersen, C. Mück-Lichtenfeld, G. Kehr and G. Erker, *Angew. Chem., Int. Ed.*, 2012, **51**, 8830–8833.
35 H. Fong, M.-E. Moret, Y. Lee and J. C. Peters, *Organometallics*, 2013, **32**, 3053–3062.
36 B. E. Cowie and D. J. H. Emslie, *Chem. – Eur. J.*, 2014, **20**, 16899–16912.
37 B. R. Barnett, C. E. Moore, A. L. Rheingold and J. S. Figueroa, *J. Am. Chem. Soc.*, 2014, **136**, 10262–10265.
38 A. J. M. Miller, J. A. Labinger and J. E. Bercaw, *J. Am. Chem. Soc.*, 2008, **130**, 11874–11875.
39 W. Su, T. Rajeshkumar, L. Xiang, L. Maron and Q. Ye, *Angew. Chem., Int. Ed.*, 2022, **61**, e202212823.
40 C. S. Durfy, J. A. Zurakowski and M. W. Drover, *Angew. Chem., Int. Ed.*, 2025, **64**, e202421599.
41 J. J. Kiernicki, M. Zeller and N. K. Szymczak, *J. Am. Chem. Soc.*, 2017, **139**, 18194–18197.
42 B. Wang, C. S. G. Seo, C. Zhang, J. Chu and N. K. Szymczak, *J. Am. Chem. Soc.*, 2022, **144**, 15793–15802.
43 H. Nöth and W. Rattay, *J. Organomet. Chem.*, 1986, **308**, 131–152.
44 A. K. Justice, G. Zampella, L. D. Gioia and T. B. Rauchfuss, *Chem. Commun.*, 2007, 2019–2021.
45 B. C. Manor, M. R. Ringenberg and T. B. Rauchfuss, *Inorg. Chem.*, 2014, **53**, 7241–7247.
46 N. Lalaoui, T. Woods, T. B. Rauchfuss and G. Zampella, *Organometallics*, 2017, **36**, 2054–2057.
47 H. J. Redman, P. Huang, M. Haumann, M. H. Cheah and G. Berggren, *Dalton Trans.*, 2022, **51**, 4634–4643.
48 T.-H. Yen, K.-T. Chu, W.-W. Chiu, Y.-C. Chien, G.-H. Lee and M.-H. Chiang, *Polyhedron*, 2013, **64**, 247–254.
49 S. Bontemps, H. Gornitzka, G. Bouhadir, K. Miqueu and D. Bourissou, *Angew. Chem., Int. Ed.*, 2006, **45**, 1611–1614.
50 G. Bouhadir and D. Bourissou, *Chem. Soc. Rev.*, 2016, **45**, 1065–1079.
51 T. G. Ostapowicz, C. Merkens, M. Hölscher, J. Klankermayer and W. Leitner, *J. Am. Chem. Soc.*, 2013, **135**, 2104–2107.
52 X. Wang, G. Kehr, C. G. Daniliuc and G. Erker, *J. Am. Chem. Soc.*, 2014, **136**, 3293–3303.
53 Z. Jian, S. Krupski, K. Škoch, G. Kehr, C. G. Daniliuc, I. Císařová, P. Štěpnička and G. Erker, *Organometallics*, 2017, **36**, 2940–2946.
54 K.-Y. Ye, X. Wang, C. G. Daniliuc, G. Kehr and G. Erker, *Eur. J. Inorg. Chem.*, 2017, **2017**, 368–371.
55 J. J. Kiernicki, M. Zeller and N. K. Szymczak, *Organometallics*, 2021, **40**, 2658–2665.
56 D. Seyferth and G. B. Womack, *Organometallics*, 1986, **5**, 2360–2370.
57 I. Bennour, L. Chatelain and P. Schollhammer, *Eur. J. Inorg. Chem.*, 2024, **27**, e202400061.
58 H.-M. Lin, C. Mu, A. Li, X.-F. Liu, Y.-L. Li, Z.-Q. Jiang and H.-K. Wu, *J. Coord. Chem.*, 2019, **72**, 2517–2530.
59 M. Kdider, C. Elleouet, F. Y. Pétillon and P. Schollhammer, *Molbank*, 2023, **2023**, M1719.
60 N. B. Makouf, H. B. Mousser, A. Darchen and A. Mousser, *J. Organomet. Chem.*, 2018, **866**, 35–42.
61 D. L. Hughes, G. J. Leigh and D. R. Paulson, *Inorg. Chim. Acta*, 1986, **120**, 191–195.
62 J. Messelhäuser, I.-P. Lorenz, K. Haug and W. Hiller, *Z. Naturforsch., B: J. Chem. Sci.*, 1985, **40**, 1064–1067.

63 M. C. Ortega-Alfaro, N. Hernández, I. Cerna, J. G. López-Cortés, E. Gómez, R. A. Toscano and C. Alvarez-Toledano, *J. Organomet. Chem.*, 2004, **689**, 885–893.
64 A. Al-Fawaz, S. Aldridge, D. L. Coombs, A. A. Dickinson, D. J. Willock, L. Ooi, M. E. Light, S. J. Coles and M. B. Hursthouse, *Dalton Trans.*, 2004, 4030–4037.
65 H. Song, K. Ye, P. Geng, X. Han, R. Liao, C.-H. Tung and W. Wang, *ACS Catal.*, 2017, **7**, 7709–7717.
66 J. N. Bentley, S. A. Elgadi, J. R. Gaffen, P. Demay-Drouhard, T. Baumgartner and C. B. Caputo, *Organometallics*, 2020, **39**, 3645–3655.
67 R. C. Neu, E. Y. Ouyang, S. J. Geier, X. Zhao, A. Ramos and D. W. Stephan, *Dalton Trans.*, 2010, **39**, 4285.
68 T. Wang, G. Kehr, L. Liu, S. Grimme, C. G. Daniliuc and G. Erker, *J. Am. Chem. Soc.*, 2016, **138**, 4302–4305.
69 M. Lindqvist, K. Borre, K. Axenov, B. Kótai, M. Nieger, M. Leskelä, I. Pápai and T. Repo, *J. Am. Chem. Soc.*, 2015, **137**, 4038–4041.
70 A.-M. Fuller, D. L. Hughes, S. J. Lancaster and C. M. White, *Organometallics*, 2010, **29**, 2194–2197.
71 D. J. Parks, W. E. Piers and G. P. A. Yap, *Organometallics*, 1998, **17**, 5492–5503.
72 D. J. Pasto, V. Balasubramaniyan and P. W. Wojtkowski, *Inorg. Chem.*, 1969, **8**, 594–598.
73 S. Dong, L. Wang, T. Wang, C. G. Daniliuc, M. Brinkkötter, H. Eckert, G. Kehr and G. Erker, *Dalton Trans.*, 2018, **47**, 4449–4454.
74 (*a*) CCDC 2451917: Experimental Crystal Structure Determination, 2025, DOI: 10.5517/ccdc.csd.cc2n9f3j; (*b*) CCDC 2451918: Experimental Crystal Structure Determination, 2025, DOI: 10.5517/ccdc.csd.cc2n9f4k; (*c*) CCDC 2451919: Experimental Crystal Structure Determination, 2025, DOI: 10.5517/ccdc.csd.cc2n9f5l; (*d*) CCDC 2451920: Experimental Crystal Structure Determination, 2025, DOI: 10.5517/ccdc.csd.cc2n9f6m.